

A high-precision magnetoencephalographic study of human auditory steady-state responses to amplitude-modulated tones

Bernhard Roß,^{a)} Christian Borgmann, and Rossitza Draganova
*Center of Biomagnetism, Institute of Experimental Audiology, University of Münster,
Kardinal-von-Galen-Ring 10, D-48129 Münster, Germany*

Larry E. Roberts
Department of Psychology, McMaster University, Hamilton, Ontario L8S 4K1, Canada

Christo Pantev
*Center of Biomagnetism, Institute of Experimental Audiology, University of Münster,
Kardinal-von-Galen-Ring 10, D-48129 Münster, Germany*

(Received 3 November 1999; revised 31 January 2000; accepted 18 May 2000)

The cerebral magnetic field of the auditory steady-state response (SSR) to sinusoidal amplitude-modulated (SAM) tones was recorded in healthy humans. The waveforms of underlying cortical source activity were calculated at multiples of the modulation frequency using the method of source space projection, which improved the signal-to-noise ratio (SNR) by a factor of 2 to 4. Since the complex amplitudes of the cortical source activity were independent of the sensor position in relation to the subject's head, a comparison of the results across experimental sessions was possible. The effect of modulation frequency on the amplitude and phase of the SSR was investigated at 30 different values between 10 and 98 Hz. At modulation frequencies between 10 and 20 Hz the SNR of harmonics near 40 Hz were predominant over the fundamental SSR. Above 30 Hz the SSR showed an almost sinusoidal waveform with an amplitude maximum at 40 Hz. The amplitude decreased with increasing modulation frequency but was significantly different from the magnetoencephalographic (MEG) background activity up to 98 Hz. Phase response at the fundamental and first harmonic decreased monotonically with increasing modulation frequency. The group delay (apparent latency) showed peaks of 72 ms at 20 Hz, 48 ms at 40 Hz, and 26 ms at 80 Hz. The effects of stimulus intensity, modulation depth, and carrier frequency on amplitude and phase of the SSR were also investigated. The SSR amplitude decreased linearly when stimulus intensity or the modulation depth were decreased in logarithmic steps. SSR amplitude decreased by a factor of 3 when carrier frequency increased from 250 to 4000 Hz. From the phase characteristics, time delays were found in the range of 0 to 6 ms for stimulus intensity, modulation depth, and carrier frequency, which were maximal at low frequencies, low intensities, or maximal modulation depth. © 2000 Acoustical Society of America. [S0001-4966(00)04708-1]

PACS numbers: 43.64.Ri, 43.64.Qh, 43.64.Yp [LHC]

INTRODUCTION

Depending upon the time course of the auditory stimulation, cerebral-evoked responses can be generally classified as transient or steady state. Responses evoked by auditory stimuli that are presented at interstimulus intervals long enough to allow intervening brain activity to subside are called transient-evoked responses.¹ If the interstimulus interval is shortened such that successive responses begin to overlap, a more complex compound response is generated. This response is referred to as a steady-state response (SSR).^{2,3} Regan⁴ has described the SSR as responses “whose constituent discrete frequency components remain constant in amplitude and phase over an infinitely long time period” (p. 35). Despite an increasing number of animal^{5–9} and human^{10–18} studies of the SSR during the last 15 years, there is still no general agreement with respect to the mechanisms or neural sources underlying SSR genesis. A cortical origin of the SSR

seems most probable, although subcortical contributions from polysensory thalamic areas can not be excluded. Epidural recordings taken from the temporal cortex of rats and cats^{5,8,19–21} are consistent with the conclusion that steady-state potentials evoked by auditory stimuli arise within the auditory cortex. Epidural recordings in humans^{22,23} and electroencephalographic (EEG) and magnetoencephalographic (MEG) field patterns evoked by auditory stimuli^{11,12,15,24–26} also suggest an active source for the auditory SSR in the supratemporal plane.

The stimuli most often used for eliciting the SSR are click trains, trains of short tone bursts, or amplitude modulated tones. Because the SSR is a periodic waveform, it has harmonic structure and can be characterized by the response parameters amplitude and phase. These response parameters depend strongly on stimulus parameters such as the stimulus rate or modulation frequency, stimulus intensity, carrier frequency, and modulation depth. This dependence is usually described by input–output characteristics (IOCs) which depict response amplitude or phase as stimulus parameters are

^{a)} Author to whom correspondence should be addressed. Electronic mail: bernhard.ross@ieec.org

manipulated over their dynamic range. Unfortunately, in all previous SSR studies conducted in humans, IOCs for different stimulus and response parameters have been determined for the most part on different subjects, owing to the impracticality of measuring multiple IOCs in the same subject within a single experimental session. A qualitative description of IOCs has been gained by this method, but a precise description of the neural dynamics underlying SSR generation requires measurement of IOCs within the same subjects and has heretofore been lacking.

The goal of the present study was to measure a range of IOCs within the same subjects, for auditory SSRs elicited by amplitude-modulated pure tones and recorded by MEG. IOCs relating SSR amplitude and phase to the stimulus parameters modulation rate, modulation depth, stimulus intensity, and carrier frequency were investigated. To overcome limitations of previous research imposed by session length, multiple sessions (16 per subject) were used. In addition, IOCs were based, not only on direct measurements of SSR amplitude and phase, but also on measurements of the behavior of cortical sources underlying SSR generation as estimated by the method of source space projection. An important advantage of this approach is that the activity of cortical sources estimated by source space projection are not affected by millimeter variations in the placement of MEG sensors with respect to the brain that inevitably occur between recording sessions. Hence, it was possible to collapse measurements across sessions, so that a high signal-to-noise ratio was achieved for each subject tested.

I. METHODS

A. Subjects

Four female and four male right-handed adults aged 22 to 32 years and free of otological or neurological disorders participated in these experiments. Normal audiological status (air conduction hearing threshold of no more than 10 dB hearing level between 250 Hz and 4 kHz) was verified by pure-tone audiometry. All subjects were right-handed according to the Edinburgh handedness questionnaire.²⁷ Informed consent was obtained from each subject after explaining to her/him the nature of the study. The experimental procedures were conducted in accordance with the Ethics Commission of the University of Münster and the Declaration of Helsinki. Subjects were paid for their participation.

For each subject, 16 experimental sessions of 1-h measurement time were scheduled. No more than two sessions per day were carried out with a half-hour break in between.

B. Stimulation

Sinusoidal amplitude-modulated (SAM) tones were continuously presented during an interval of 200 s. The SAM waveform $y(t)$ was defined by

$$y(t) = a \cdot \sin(2\pi f_c t) \cdot (1 - m \cos(2\pi f_m t)), \quad (2.1)$$

in which a denoted the amplitude of the signal, f_c denoted the carrier frequency, and f_m the modulation frequency. The last term describes the signal's envelope. The modulation depth m is equal to the ratio $(y_{\max} - y_{\min}) / (y_{\max} + y_{\min})$,

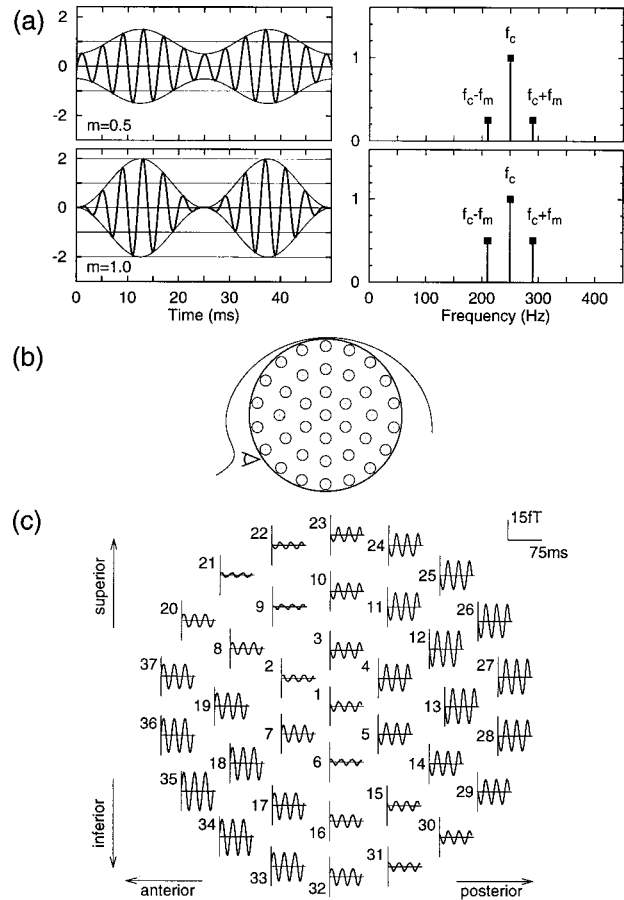


FIG. 1. (a) Time series and amplitude spectrum of sinusoidal modulated tones for modulation depth $m=0.5$ and $m=1$; (b) schematic of the sensor placement over the left hemisphere; and (c) waveforms of magnetic field obtained from 37 channels.

where y_{\max} and y_{\min} are the maximum and minimum of the waveform's envelope, respectively. The modulation depth ranged from zero to 1, and was expressed in percent. Resolving the sine-cosine product into a sum of terms yields the spectral representation of the SAM signal

$$y(t) = a \sin(\omega_c t) - m \frac{a}{2} \sin(\omega_1 t) - m \frac{a}{2} \sin(\omega_2 t), \quad (2.2)$$

which consists of three distinct spectral lines at $\omega_c = 2\pi f_c$, $\omega_1 = 2\pi(f_c - f_m)$, and $\omega_2 = 2\pi(f_c + f_m)$. Both the time series and the amplitude spectrum of the stimulus signal are shown in Fig. 1(a). The dependencies of the SSR on the four stimulus parameters, f_m , f_c , a , and m , were investigated in this study. Only integer values in Hz were chosen for the carrier frequency as well for the modulation frequency. Therefore, 1 s was a common multiple of the periodicity of $y(t)$ for all combinations of f_c and f_m , and permitted calculation of the stimulus waveform for periods of 1-s duration. The software for stimulus calculation and presentation, and the graphical user interface for controlling the experiments, were run on a Sun SPARC computer which also served as the front end for data acquisition. A 16-bit digital-to-analog converter (ADDA1418, Analyx, Inc.) was used to convert the stimulus waveform into an audio signal at a rate of 20 000 samples/s. A trigger at the onset of each 1-s stimulus

period was provided by the stimulus device for synchronization with the data acquisition system.

Magnetically silent delivery of the stimuli was provided by a special sound delivery system consisting of speakers (1 in. compression driver, Renkus-Heinz Inc.) mounted outside the magnetically shielded room which were connected to a silicon ear piece through 6.3 m of echo-less plastic tubing (16 mm inner diameter). The frequency characteristic of this system deviated less than ± 10 dB between 200 and 6000 Hz. Since the stimulus was defined in a frequency band no wider than 200 Hz width, stimuli were not distorted by the frequency characteristic of the sound delivery system. The transmission delay of about 19 ms was compensated by an appropriate shift of the trigger signal. Before carrying out the experiments, both the signal spectrum of the stimulus and its correct timing were checked by means of a 2-cm³ ear simulator (Brüel & Kjør model 4157) that was equipped with an 1/2" condenser microphone (Brüel & Kjør model 4134) and connected to the silicon ear piece at the end of the sound delivery system.

Four experiments were carried out in which auditory evoked steady-state responses were investigated in detail while stimulus intensity, carrier frequency, modulation frequency, and the modulation depth were manipulated. Within experimental sessions these stimulus parameters were varied one at a time while the others were kept constant. In all experiments the stimuli were presented continuously for 200 s monaurally to the subject's right ear. Stimulus intensity was referred to the individual sensation threshold. For this purpose, the subject's hearing threshold was measured prior to each experimental session by applying tonebursts of 500 ms duration of the relevant stimulus type through the sound delivery system.

1. Stimulus intensity

In order to obtain an optimal signal-to-noise ratio, the carrier frequency f_c of the SAM stimulus signal was set to 250 Hz, and the modulation depth m to 100%. The modulation frequency f_m was set to 39 Hz instead of 40 Hz because 39 Hz had no common factor with the power-line frequency of 50 Hz. The SAM stimulus signal was presented at seven intensity steps of 10 dB each, ranging from 30- to 90-dB sensation level (SL). Each intensity was presented at least twice. For the two lowest intensity steps (30- and 40-dB sensation level), a smaller response amplitude was expected. Therefore, these intensities were repeated four times, in order to increase the signal-to-noise ratio. For each subject, three experimental sessions of 1 h each were carried out.

2. Modulation depth

For the investigation of the effect of changing modulation depth on the SSR amplitude, SAM stimuli with $f_c = 250$ Hz, $f_m = 39$ Hz at an intensity of 70-dB sensation level were presented. The modulation depth m was changed from 100% to 10% in 10%-steps, and additionally $m = 5\%$ was investigated. The stimuli were presented twice for 200 s at $m \geq 30\%$ and four times at $m \leq 20\%$. Four sessions of 1-h duration each were carried out for each subject.

3. Carrier frequency

The carrier frequency of the SAM-tone signal was investigated at 250, 500, 1000, 2000, and 4000 Hz with a constant modulation frequency of $f_m = 39$ Hz, a modulation depth of 100%, and an intensity of 70-dB sensation level. Experimental blocks of 200-s duration were repeated five times in random order within three experimental sessions.

4. Modulation frequency

The effect of modulation frequency on the SSR was investigated between 10 and 48 Hz in steps of 2 Hz, and between 55 and 100 Hz in steps of 5 Hz. The power-line frequency (50 Hz) and its harmonics and subharmonics were excluded from the study to avoid line frequency noise. Ninety-eight Hz was included as an alternative for 100 Hz. Thus, a total of 30 different modulation frequencies was investigated. The carrier frequency was set to 250 Hz, the modulation depth to 100%, and the intensity to 70-dB sensation level. At the beginning of each experimental session, the hearing threshold was determined at $f_m = 39$ Hz. Stimulus amplitudes were kept constant when changing the modulation frequency. Each stimulus was presented at least twice for 200 s, and the different stimuli were presented in random order. For each subject, six sessions of 1 h each were carried out.

C. Data acquisition

Recordings were performed in a magnetically and acoustically shielded room. The subjects rested in right lateral position on a vacuum cast, with their heads lying on molds to permit stable fixation throughout the whole experimental session.

The MEG was recorded with a 37-channel neuromagnetometer (MAGNES, Biomagnetic Technologies). The detection coils of the neuromagnetometer were arranged in a circular concave array with a diameter of 144 mm and a spherical radius of 122 mm. The distance between the centers of the coils was 22 mm; the coil diameter was 20 mm. The sensors were configured as a first-order axial gradiometer with a baseline of 50 mm. The spectral density of the intrinsic noise of each channel was between 5 and 7 fT/ $\sqrt{\text{Hz}}$ in the frequency range above 1 Hz.

The sensor array was placed over the left temporal plane, centered over a point about 1.5 cm superior to the position T3 of the 10–20 system for electrode placement, as close to the subject's head as possible [Fig. 1(b)]. A sensor-position indicator system determined the spatial locations of the sensors relative to the head and indicated if head movements occurred during the recordings. No head movements sufficient to require discarding of data were observed in the study. During the MEG session, subjects watched cartoon videos that were projected via fiber cable optic into a non-magnetic display in order to fixate their attention. The subjects were instructed to stay in a relaxed state to reduce the influence of myogenic activity on the MEG signals and their compliance was verified by video monitoring. The reason for

maintaining wakefulness was that substantially decreased SSR amplitudes during sleep have previously been reported.²⁸

During the experimental blocks of 200 s, 37 channels of magnetic field data (bandwidth from 1 to 200 Hz, sampling rate 520 Hz, resolution 16 bits) were continuously recorded with stimulus triggers and stored for off-line analysis.

D. Data analysis

1. Amplitude and phase of the SSR

The data analysis was a threefold procedure involving data reduction and enhancement of the signal-to-noise ratio. First, the data stream of 200-s duration was split into segments of 1 s each, starting at the onset of the trigger signal. These segments were averaged in the time domain. Segments with signal variations of more than 3 pT were considered to contain artifacts and were rejected on a single-channel basis. This first step of data analysis reduced the amount of data by a factor of 200 and improved the signal-to-noise ratio by a factor of up to $\sqrt{200}$. The second step of the data analysis collapses the time series of the 37 MEG sensors into a single-channel signal in order to achieve an improved signal-to-noise ratio as compared to each of the 37 input signals. The method that was used (called ‘‘source space projection’’) estimates the activity in a certain brain area by linear combination of activities measured outside the brain. The resulting signal is a time series of the magnetic dipole moment. It reaches maximum values only for the typical dipolar magnetic field pattern of a single current source in a previously specified brain region. Therefore, the method is spatial sensitive. Spontaneous brain activity from other regions is diminished by source space projection. In addition, uncorrelated system noise is canceled out which otherwise would be a limiting factor for measuring frequencies above 40 Hz. The source space projection method is based on the linear relationship that exists between each current source $\mathbf{q}(\mathbf{R})$ at the source positions \mathbf{R} in the brain and the magnetic field $b_i(\mathbf{r})$ which is measured with the i th sensor at position \mathbf{r} outside the head. This relation is given by the equation $\mathbf{b}(\mathbf{r}) = \mathbf{L}(\mathbf{r}, \mathbf{R}) \cdot \mathbf{q}(\mathbf{R})$.²⁹ The lead field matrix $\mathbf{L}(\mathbf{r}, \mathbf{R})$ depends on the source position and the sensor position, as well as upon the properties of the volume conductor and the sensors. In general, the described relation maps each current source into a multidimensional *signal space*.³⁰ Vice versa, a linear spatially and orientation selective filter can be derived as a projection operator in signal space, which does a reverse mapping into the source space. The filter output signal is a waveform that would be seen by a *virtual sensor*³¹ which responds maximally to the region of interest in the brain, attenuating signal from other regions or signals with different source current direction. Such a filter is the dot product of the measured magnetic field $\mathbf{b}(\mathbf{r})(t)$ with a weighting vector $\mathbf{W}(\mathbf{q}(\mathbf{R}))$.³²

In this study, the pseudo inverse $\mathbf{L}^{-1}(\mathbf{r}, \mathbf{R})$ of the lead field matrix and the assumed orientation $\mathbf{q}(\mathbf{R})/|\mathbf{q}(\mathbf{R})|$ of the underlying source were used to define the filter \mathbf{W} . Using the model of a single dipole in a homogeneous sphere, the waveform $\hat{q}(t)$ of magnetic dipole moment was calculated by

$$\hat{q}(t) = \mathbf{b}(\mathbf{r})(t) \cdot \mathbf{L}^{-1}(\mathbf{r}, \mathbf{R}) \cdot \mathbf{q}(\mathbf{R}) / |\mathbf{q}(\mathbf{R})|. \quad (2.3)$$

Therefore, units of measurement which depend on the position of the sensor (magnetic field in fT) were transformed into a source strength estimate (dipole moment in nA·m) that did not depend on the slightly different positions of the measurement system with respect to the subject’s head during the multiple sessions.

The third step in the data analysis was the calculation of the amplitude and phase of the spectral components of $\hat{q}(t)$ at the modulation frequency and some of its harmonics. The results were used to calculate the input–output characteristics (IOCs) for the different stimulus conditions. From the $N=520$ data points of the magnetic dipole moment $\hat{q}(i)$, the discrete Fourier coefficients at the frequency k were calculated by

$$a(k) = \frac{2}{N} \sum_{i=1}^N \hat{q}(i) \sin \frac{ik}{N} \omega_k, \quad (2.4)$$

$$b(k) = \frac{2}{N} \sum_{i=1}^N \hat{q}(i) \cos \frac{ik}{N} \omega_k. \quad (2.5)$$

The discrete calculation of Fourier coefficients, which is also known as quadrature demodulation, had the advantage that amplitudes of the spectral components of $\hat{q}(i)$ were calculated at the exact frequencies of interest even when the number of data points (520) did not equal an integer power of 2. The phase of the SSR is usually measured with respect to the zero-phase angle of a sine approximation to the response waveform.³³ A delayed sine wave (positive time shift) has negative zero phase. Therefore, an increasing delay of the response waveform results in a negative increasing phase value if the carrier and modulation frequencies do not change. The phase $\varphi(f)$ was calculated from the complex Fourier coefficient at frequency f considering the signs of the real and imaginary parts, and was hence defined on the interval $[-\pi, \pi)$. In order to keep $\varphi(f)$ monotonically decreasing, -2π was added to it when needed.

For the analysis of the effect of modulation frequency on SSR phase, the group delay τ was calculated as

$$\tau(f_0) = - \frac{1}{2\pi} \left. \frac{\partial \varphi}{\partial f} \right|_{f_0}. \quad (2.6)$$

In a linear system the group delay $\tau(f_0)$ has the meaning that a group of frequencies centered around f_0 is delayed by $\tau(f_0)$ in the sense that its contribution to the impulse response $h(t)$ is maximum at $\tau(f_0)$.³⁴ In the context of SSR analysis, $\tau(f_0)$ is often called the *apparent latency*.⁴

2. The SSR waveform

The stationary part of power-line frequency noise (multiples of 50 Hz) was calculated by the discrete Fourier transform and, after time-series expansion, was subtracted from the waveform of the magnetic dipole moment. After the line frequency noise was thus eliminated, subsequent sections of length equal to one period of the modulation frequency f_m were averaged and formed one period of the time series of

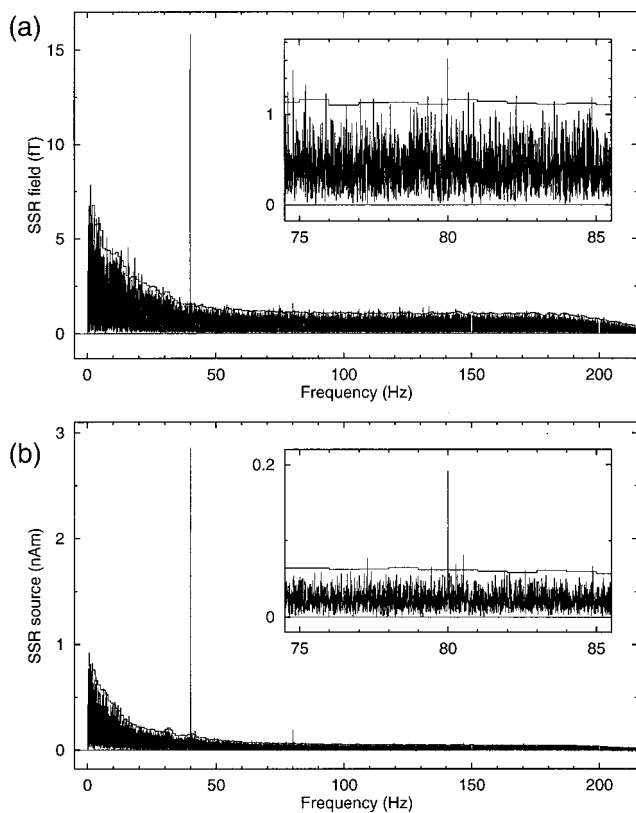


FIG. 2. (a) Amplitude spectrum of the magnetic field obtained from the maximally responding sensor channel; (b) amplitude spectrum of the source waveform after source space projection. Enlarged displays of both spectra are shown in the insets for a 10-Hz frequency range centered at 80 Hz. The thin horizontal lines denote the 99%-confidence limits (2.33 times the standard deviation) for response detection.

the SSR. Linear interpolation between sampled data points was necessary because $1/f_m$ did not equal an integer number of sampling intervals. Thus, the waveform of the SSR, which was measured for a total epoch length of T s, was the result of averaging of $N = T \cdot f_m$ stimulus related epochs. The number of averaged epochs, and, correspondingly, the improvement of the signal-to-noise ratio as well, depended on the modulation frequency and ranged from $N=2000$ at 10 Hz to $N=18\,600$ at 98 Hz. In contrast, these properties of data analysis in the frequency domain were independent of f_m , and the signal-to-noise ratio was improved evenly over the whole frequency range. For this reason, the waveforms of the SSR were calculated for visualization purpose only.

3. Spectral analysis

Source space projection was also applied to the raw (nonaveraged) data, and time series of magnetic moment ($200 \text{ s} \times 520 \text{ samples/s} = 104\,000 \text{ samples}$) were calculated. High-resolution amplitude spectra were obtained from these time series by Fourier transform, giving 200 lines per Hz. Examples of the high-resolution amplitude spectrum are shown in Fig. 2 for the magnetic field data [panel (a)] and the dipole moment data [panel (b)], respectively. The purpose of this analysis was to estimate the non-stimulus-locked MEG background activity. Both the evoked-response amplitudes and the line frequency noise were expected to be concentrated around integer frequencies. Therefore, for each fre-

quency bin starting at the integer frequency f_i between 1 and 200 Hz, the mean power was calculated from 180 spectral lines in the interval from $f_i + 0.05 \text{ Hz}$ to $f_i + 0.95 \text{ Hz}$. The square root of the mean power gave an estimate of the standard deviation $\sigma_n(f)$ of the MEG background noise. For a measured response amplitude $a(f)$ at the frequency f , the signal-to-noise ratio $\text{SNR}(f)$ was defined as the ratio $\text{SNR}(f) = a(f)/\sigma_n(f)$. The value of $2.33\sigma_n$ was calculated for all frequency bins as an estimate of the 99%-confidence level for the detection of response signal amplitudes (Fig. 2). SSRs with amplitudes below the confidence level were rejected from further data analysis.

4. Source localization

A prerequisite for the source space projection was the estimation of the position \mathbf{R} and the orientation $\mathbf{q}(\mathbf{R})/|\mathbf{q}(\mathbf{R})|$ of the underlying sources in a head-based coordinate system. In principle, either anatomical information or results from MEG source estimation carried out on the actual data could be used. The latter was the case in this study.

The origin of the head-based coordinate system was set at the midpoint of the mediolateral axis (y axis) which joined the center points of the entrances to the acoustic meatii of the left and right ears (positive towards the left ear). The postero–anterior axis (x axis) was oriented from the origin to the nasion (positive towards the nasion) and the inferior–superior axis (z axis) was perpendicular to the x – y plane (positive towards the vertex).

Magnetic field data epochs corresponding to single periods of the modulation signal were averaged, and the point of time at which the global field power (the mean square sum over all MEG channels) reached its maximum was determined. At this time point the field of a single moving dipole was fitted to the averaged data in order to estimate the magnetic source localizations. A homogeneous spherical model was used for the dipole fits. The shape of each subject's head was digitized during preparation of the experiments, and the best-fitting sphere to the curvature of the head above the estimated source was calculated. For each subject and experimental condition, the median values of the estimated source coordinates and dipole orientations were used as a reference for the source space projection. In contrast to the magnetic field data $\mathbf{b}(\mathbf{r})$, which depend on the position of the sensor array relative to the subject's head, the magnetic moment data $\hat{q}(t)$ refer to a fixed area in the head only. Therefore, the time series of the magnetic moment was a measure which enabled the comparison of data from subsequent experimental sessions without requiring any precise repositioning of the MEG sensor array.

5. Grand averages

IOCs were obtained for all single subjects and all experimental conditions and were grand averaged over all subjects for each experimental condition. In order to reduce the influence of interindividual variations, the individual IOCs were scaled to unity at an appropriate value of the stimulus parameter. In addition, the mean phase was subtracted from individual phase characteristics. The 99%-confidence interval of

each grand average was calculated by the bootstrap resampling method.³⁵ The modulation frequency IOC was smoothed by weighted averaging over adjacent values by the function $\bar{x}_i = 0.2x_{i-1} + 0.6x_i + 0.2x_{i+1}$.

II. RESULTS

Steady-state responses with amplitudes statistically significantly different from MEG background activity were detected at the modulation frequency of the auditory stimulus and some of its harmonics as well for all subjects and all experimental conditions. No peaks of oscillatory MEG activities at other frequencies were observed in the frequency range from 1 to 200 Hz.

A. Example of individual data

The 37-channel SSR data obtained from Subject A0010 when steady-state stimulation ($f_c = 250$ Hz, $f_m = 40$ Hz, and $m = 100\%$) was applied at 70 dB_{SL} are displayed in Fig. 1(c). The measured magnetic field reveals a pronounced dipolar pattern with a polarity reversal between posterior and anterior channels. The field distribution reaches its posterior maximum in channel 27 with an amplitude of 16 fT. The amplitude spectrum of this channel, which is shown in Fig. 2(a), consists of a distinct spectral line at the modulation frequency and smaller lines at its harmonics, and the MEG background activity, which is widely spread over the whole frequency range. The MEG background spectrum reveals a $1/f$ -shape for low frequencies and approaches a minimum constant spectral density near 50 Hz. The spectral power above 50 Hz represents mainly measurement system noise, which is reduced above 200 Hz by the antialiasing low-pass filter. The standard deviation of the background noise is 0.5 fT, which equals the sensor noise (7 fT/ $\sqrt{\text{Hz}}$) divided by the square root of the length of the time window ($\sqrt{200}$ s).

Figure 2(b) displays the SSR spectrum after source space projection, where a reduction of the MEG background activity is evident. Although Figs. 2(a) and 2(b) are on different scales (fT or nA·m, respectively) the dimensionless SNR allowed a quantitative comparison. The SNR was enhanced by a factor of 1.5 at 10 Hz, by a factor of 2 at 50 Hz, and by a factor of 4 at 100 Hz and above. The intersection point between the low-frequency range in which the brain activity is mostly prevalent and the frequency range which contains mostly system noise shifted from about 50 Hz to about 100 Hz with source space projection. The SSR corresponding to the modulation frequency was again represented by a single spectral line at 40 Hz after source space projection. However, the spectral peak at the second harmonic (80 Hz) was enhanced compared to the untransformed field [Fig. 2(a)]. The frequency range around 80 Hz in both data sets is shown with enlarged scale in the insets of Figs. 2(a) and 2(b), with the thin horizontal line denoting the 99%-confidence level. In the untransformed data, the spectral line at 80 Hz exceeds this level with a SNR of 3.32 [Fig. 2(a)] compared to a SNR of 7.45 after source space projection [Fig. 2(b)]. The SNR at 40 Hz was increased by a factor of 1.88 from 24.5 to 46.0.

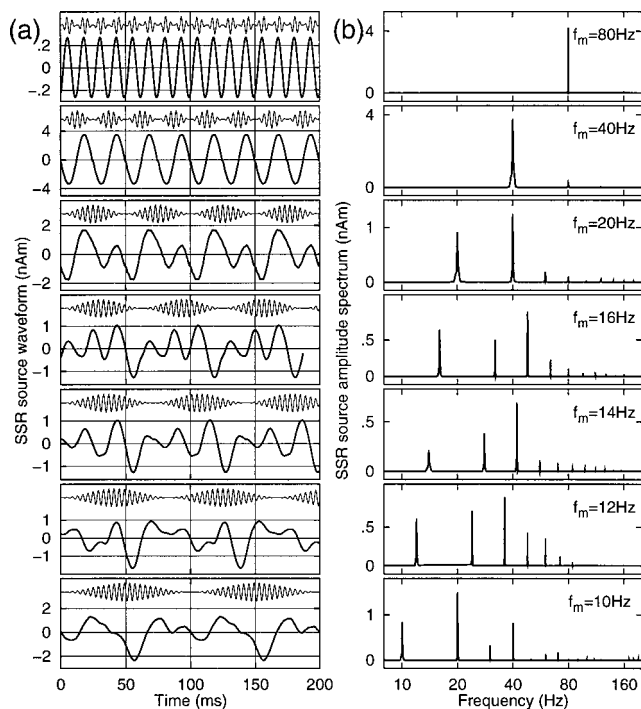


FIG. 3. Examples of individual SSR data; (a) Source waveforms obtained with sinusoidal amplitude modulated tones ($f_c = 250$ Hz, $m = 100\%$, 70 dB) at various modulation frequencies. Thin lines represent the stimulus waveforms. (b) Corresponding amplitude spectra of the source waveforms.

B. Source localization

Although source analysis of the human auditory SSR was not the objective of this study, source localization was a prerequisite for the source space projection procedure. The grand average of the median values of the estimated source coordinates of the eight subjects was 1.29 cm in the posterior–anterior direction (x), 4.30 cm in the mediolateral direction (y), and 6.12 cm in the inferior–superior direction (z). When the carrier frequency was varied between 250 and 4000 Hz, a tonotopic cortical representation was found which extended over a range of 5 mm in the mediolateral direction, with higher frequencies situated closer to the sagittal midline.¹⁵

C. Modulation frequency

As reported above, a clearly detectable SSR was observed at each tested modulation frequency in every subject. The source waveforms of the SSR for Subject A0010 at various modulation frequencies are shown in the left panel of Fig. 3. SAM stimulus signals are also depicted at each modulation frequency. At 10 Hz, the lowest modulation frequency, the response waveform consisted of a number of positive and negative deflections which repeated periodically corresponding to the stimulation rate. Increasing the modulation frequency reconfigured the SSR source waveform, and at about 40 Hz and above, the waveform revealed an almost sinusoidal shape. At modulation frequencies below 40 Hz, deflections occurring at the same latency as obtained from the 40-Hz response could be identified for most waveforms with respect to the rising edge of the stimulus signal. At modulation frequencies of 10 to 40 Hz, all waveforms exhibited a

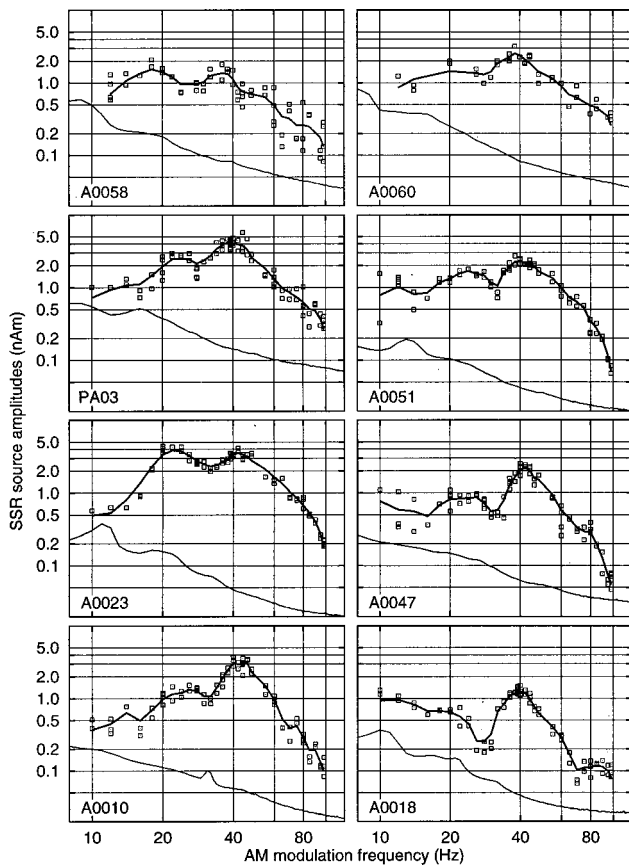


FIG. 4. SSR amplitudes versus modulation frequency for all subjects. The square symbols denote the results from single measurements of 200-s duration. The thick lines represent a smoothed average over single measurements. Thin lines denote the standard deviation of the MEG background activity.

negative (downward) deflection at 56 ms. For f_m of 12 to 40 Hz, a positive (upward) deflection occurred at 44 ms, whereas a negative deflection at 31 ms was observed for f_m of 14 to 40 Hz, and so on.

A more quantitative description of the SSR at various modulation frequencies is given by the Fourier expansions of the source waveforms displayed in the right panel of Fig. 3. The spectrum, corresponding to $f_m = 10$ Hz, demonstrated a clear component at f_m , but the amplitude of the second harmonic (20 Hz) was almost double in size. The spectral component of the SSR at 40 Hz had about the same amplitude as the fundamental 10-Hz component. The SSR evoked by $f_m = 12$ Hz consisted of a component at 12 Hz, a somewhat bigger component at 24 Hz, a most prominent component at 36 Hz, and components with decreasing amplitudes above 40 Hz. The spectrum of the SSR at $f_m = 14$ Hz had a dominant peak at the third harmonic (42 Hz), which was twice the size of the second harmonic (28 Hz) and four times the size of the fundamental (14 Hz). At $f_m = 16$ Hz, the third harmonic (48 Hz) of the SSR was more pronounced than the fundamental. When the stimulus was modulated with $f_m = 20$ Hz, the SSR spectrum showed its largest peak at the second harmonic (40 Hz). In contrast, the SSR spectrum at $f_m = 40$ Hz was dominated by the fundamental peak, which was 17.3 times bigger than the second harmonic (80 Hz). Nevertheless, the amplitude of the peak at 80 Hz was measured with high accuracy

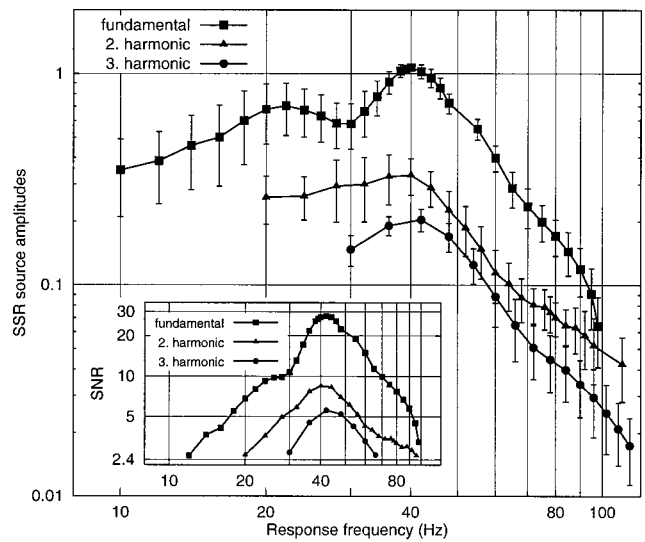


FIG. 5. Normalized spectral amplitudes of SSR at the modulation frequency and second and third harmonic as grand averages over eight subjects. The error bars denote the 99%-confidence interval obtained from bootstrap resampling. The inset displays the corresponding signal-to-noise ratio characteristics.

and was 7.5 times the standard deviation of the background noise. The 80-Hz response spectrum showed a single peak at the fundamental frequency only (the amplitude of the second harmonic was not significantly different compared to the background noise).

IOCs describing the relation between the magnitude of the response and the modulation frequency are widely known as modulation transfer functions (MTFs). MTFs are presented in Fig. 4 (thick lines) for each of the eight subjects. The thin lines denote the standard deviation of the background MEG amplitude spectrum. In some cases, at frequencies below 20 Hz the fundamental amplitudes did not reach the significance level of 2.33 times the standard deviation ($p \leq 0.01$). However, because the second or higher harmonics exceeded the significance level, these frequencies were not excluded from further analysis. Inspection of Fig. 4 shows that MTFs peaked around 40 Hz in each subject, with amplitude varying between 1 and 4 nA·m among the subjects. A second peak around 20 Hz was also seen in all subjects, although the ratio of the 20-Hz peak to the 40-Hz peak differed between subjects. For two subjects (A0023 and A0058), the 20-Hz and 40-Hz peaks reached the same size; for all other subjects the 20-Hz peak was smaller than the 40-Hz peak.

In order to reduce the between-subject variation before calculating the grand average MTF, individual MTFs were scaled, setting the mean amplitude to unity in the frequency range of 36 to 44 Hz. The resulting grand average MTF is shown in Fig. 5. The 99%-confidence interval obtained from bootstrap resampling also is added. The amplitude characteristic showed a significant peak around 40 Hz. In contrast, the 20-Hz peak, which was clearly pronounced in some subjects, did not reach significance in the grand average. Above 40 Hz, the MTF decreased with increasing modulation frequency and followed a linear slope (18 dB/octave) in a log-log scaled diagram. Additionally, the frequency characteris-

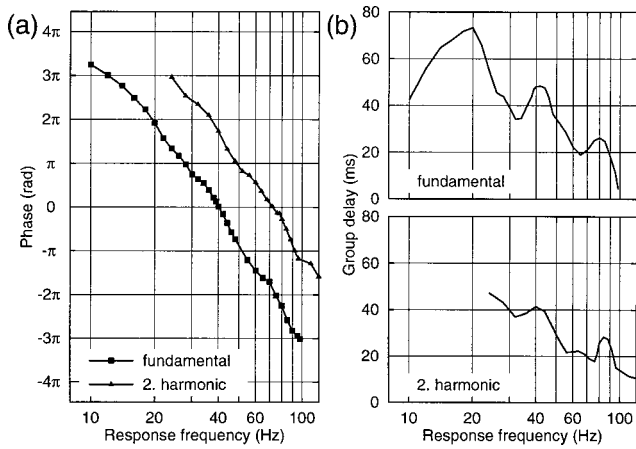


FIG. 6. (a) Phase characteristics of SSR at the modulation frequency and the second harmonic (shifted 2π upwards for clarity); (b) group delay (apparent latency) obtained from the phase characteristics of the fundamental and second harmonic response.

tics of the second and third harmonic of the SSR are shown in Fig. 5 (e.g., the third harmonic at 42 Hz is a response to 14-Hz stimulation). Both characteristics reached maximum values around 40 Hz and decreased for higher frequencies. Between 40 and 80 Hz, the shape of both characteristics was similar to the characteristic of the fundamental SSR amplitude. Above 80 Hz the variability increased due to the lower signal-to-noise ratio. The inset of Fig. 5 shows the MTF in relation to the MEG background activity (signal-to-noise ratio, SNR). This graph demonstrates that in terms of SNR the second harmonic of the SSR is predominant over the fundamental in the modulation frequency range between 10 and 20 Hz. Also, the SNR of the third harmonic is higher than the fundamental SSR in the modulation frequency range between 10 and 15 Hz.

The modulation frequency-phase IOC is shown in the left panel of Fig. 6 for the fundamental SSR, and for its second harmonic as well. Since the absolute phase angle is uncertain for additional multiples of 2π , the phase characteristic of the second harmonic was shifted by 2π upwards for the reason of clarity. Both characteristics showed similar shapes, decreasing monotonically with increasing modulation frequency. In order to obtain the corresponding group delay (apparent latency), the first derivative of the phase characteristic was calculated and displayed in the right panel of Fig. 6. Both the group delay of the fundamental SSR and of the second harmonic tended to shift toward shorter delays with increasing modulation frequency. The group delay IOC of the fundamental SSR showed three distinct peaks at 20, 40, and 80 Hz with apparent latencies of 72, 48, and 26 ms, respectively. The IOC for the second harmonic also suggested peaks around 40 and 80 Hz with group delay values in the same range.

D. Stimulus intensity

The effect of stimulus intensity on the SSR was investigated with a carrier frequency of 250 Hz and the modulation rate set to 39 Hz. For all subjects, an increase in SSR amplitude with increasing intensity was observed. In order to re-

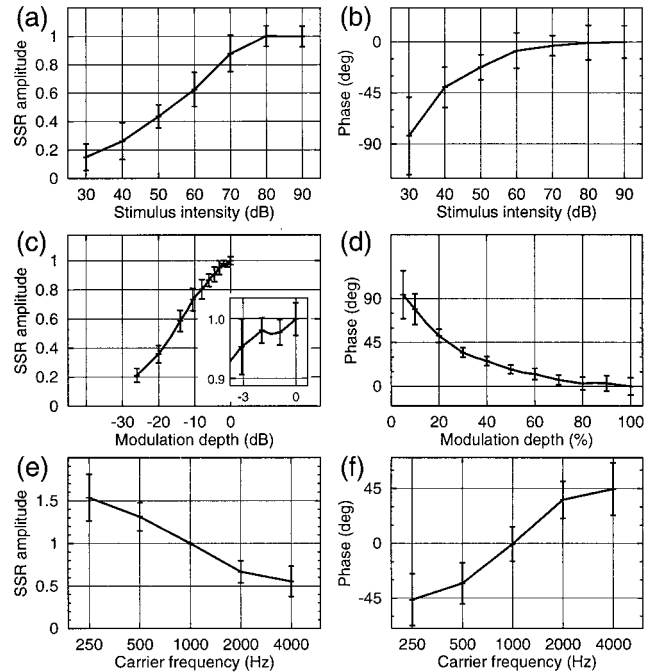


FIG. 7. Amplitude- and phase characteristics of SSR at the modulation frequency obtained by averaging over eight subjects (a), (b) as function of the stimulus intensity (c), (d) as function of the modulation depth, and (e), (f) as function of the carrier frequency. The error bars denote the 99%-confidence interval obtained from bootstrap resampling.

duce between-subject variation, the amplitude values of each subject were scaled by the observed mean response amplitude in the 80- to 90-dB stimulus intensity range. The scaled SSR amplitudes were averaged over the eight subjects, and 99%-confidence intervals were calculated by the bootstrap resampling method. The resulting SSR intensity-amplitude IOC [Fig. 7(a)] was almost linear in the intensity range from 40 to 70 dB. The IOC reached its maximum value at 80-dB stimulus intensity, and no further increase was obtained with an intensity of 90 dB. Therefore, all following experiments were carried out at the intensity of 70-dB sensation level.

In order to calculate the stimulus intensity-phase IOC, the individual mean phase for each subject was subtracted first. The phase data were then averaged over the eight subjects and the 99%-confidence intervals were calculated. Finally, the phase value at 90 dB, which represented the highest intensity, was fixed to zero. The resulting stimulus intensity-phase IOC is shown in Fig. 7(b). Phase increased with increasing intensity, corresponding to a shorter delay at higher intensity. For the 30-dB sensation level, an average phase of $\pi/2$ was obtained and corresponded to a delay of 6 ms compared to the SSR at 90-dB sensation level. For all eight subjects, delay time was shorter at the highest intensity of 90 dB than the lowest intensity of 30 dB.

E. Modulation depth

All subjects showed a decrease in SSR amplitude when the modulation depth was reduced. In order to diminish the effect of between-subject variation, each individual IOC was transformed to a relative scale by setting the amplitude obtained at $m = 100\%$ to 1. The modulation depth-amplitude

IOC averaged over the eight subjects is displayed in Fig. 7(c). The modulation depth is given on a dB scale referenced to $m=100\%$, whereas the amplitude is given on a linear relative scale. In order to facilitate comparison between Figs. 7(c) and 7(a), the axes of both figures are scaled at the same size. The two characteristics showed little variation when m was changed between 100% and 80% (-2 dB) but decreased linearly when modulation depth was varied between 80% and 5% (-2 to -26 dB).

Alternatively, modulation depth can be described as a stimulus with constant carrier amplitude but with sideband amplitudes that change proportionally to m [cf. Fig. 1(a)]. Following this interpretation, the modulation depth-amplitude IOC decreased linearly when the sideband intensity decreased on a dB scale. The SSR amplitude decreased by a factor of 3, from $m=80\%$ to $m=8\%$ (corresponding to a 20-dB intensity variation). For comparison, the SSR amplitude decreased only by a factor of 2 when stimulus intensity changed from 70 to 50 dB at constant modulation depth of 100%. Thus, the slope of the modulation depth-amplitude IOC appeared to be steeper than the slope of the amplitude intensity IOC.

In contrast to the effect of stimulus intensity on the phase angle, all subjects showed an increasing delay with increasing modulation depth. The modulation depth-phase IOC, which is shown in Fig. 7(d), was calculated in the same way as the amplitude intensity characteristic.

F. Carrier frequency

In order to reduce the effect of between-subject variability in the absolute values of SSR amplitude, relative amplitude variations were referred to the SSR amplitude for the 1000-Hz carrier frequency. Five of the seven subjects participating in this experiment showed a monotonic decrease of the SSR amplitude when the carrier frequency was changed from 250 to 4000 Hz, whereas two subjects showed monotonic decreases between 500 and 2000 Hz and reversed behavior at the extreme frequencies. The carrier frequency-amplitude IOC obtained by averaging over all subjects is shown in Fig. 7(e). Inspection shows that SSR amplitude decreased linearly with increasing carrier frequency on a logarithmic scale. From 250 to 4000 Hz, SSR amplitude decreased by a factor of 2.8. The corresponding phase characteristic is displayed in Fig. 7(f) and exhibited an increasing phase angle with increasing carrier frequency. This is equivalent to a time delay 6.4 ms shorter at 4000 Hz than at 250 Hz.

III. DISCUSSION

Steady-state evoked magnetic fields were detected from all subjects in all experimental conditions and were analyzed in the time and frequency domains. Representation of the fundamental of the SSR by a single spectral line without any noticeable sidelobes indicates that the SSR had a fairly stable amplitude throughout the measurement time. The mean source coordinates ($x=1.29$ cm, $y=4.30$ cm, $z=6.12$ cm) obtained for single equivalent dipoles fitted to the evoked magnetic field for each subject correspond to the grand av-

erage values of $x=1.0$ cm, $y=4.30$ cm, and $z=6.05$ cm reported in a previous study¹⁵ using queues of Gaussian tone pulses with a repetition rate of 39 Hz and a carrier frequency of 250 Hz. This correspondence suggests that the SSR was generated from sources in the primary auditory cortex. Although individual MRI data were not available to corroborate this conclusion, coregistration of SSR sources was carried out in the previous investigation¹⁵ and confirmed the presence of generators in the primary auditory cortex.

The goal of this study was to measure input-output characteristics (IOCs) relating SSR amplitude and phase to several parameters of steady-state stimulation in the same subjects. To achieve this goal, the SSR magnetic field was transformed by signal space projection into a time series representing the behavior of the cortical sources underlying SSR generation. Because the transformation was not affected by variations that occur when the MEG sensors are repositioned with respect to individual neuroanatomy during repeated sessions, the data from repeated sessions on the same subjects could be averaged. This allowed several IOCs to be investigated in these subjects with a very high signal-to-noise ratio. Signal space projection improved signal-to-noise ratios by a factor in the range of 2 to 4.

A. Modulation frequency

The data presented in this study demonstrate that the auditory cortex responds to amplitude fluctuations of SAM tones in the frequency range from 10 to 98 Hz.

The shape of the average MTF shown in Fig. 5, as well as the MTFs shown in Fig. 4 for single subjects, resemble those of a low-pass filter with an upper cutoff frequency near 50 Hz. Similar MTFs were obtained in psychophysical experiments³⁶ which measured the ability of subjects to resolve sinusoidal amplitude modulations at different modulation rates. Psychophysical MTFs describe perceptual sensitivity to AM sounds by determining just-noticeable-differences in modulation depth at different modulation frequencies. If the effects of pitch perception are eliminated either by using a wideband noise carrier³⁶ or instructing subjects to listen for "roughness" only,³⁷ the psychophysical MTF shows decreasing perceptual sensitivity by about 3 dB/octave with increasing modulation frequency above about 50 Hz. Correspondingly, an EEG study by Rees *et al.*³⁸ obtained a MTF with a slope of 3 to 6 dB/octave when modulation frequency was increased above 50 Hz. On the other hand, we found a steeper slope of 18 dB/octave above 50 Hz in the present study where MEG was measured. The difference between our findings and those of Rees *et al.* may be due to the fact that MEG measurements are sensitive only to cortical sources of brain activity. Animal data concur with this hypothesis by suggesting that the best modulation frequency for amplitude-modulated tones decreases along the auditory pathway. Best modulation frequencies of about 500 Hz have been reported for the cochlear nucleus of the gerbil,³⁹ of 100 to 120 Hz for the inferior colliculus of the rat,⁴⁰ and of more than 50 Hz in the anterior auditory field of the cat.⁴¹ Rees and Møller⁴⁰ reported further that the frequency of the maximum response and the upper cutoff frequency of MTFs obtained from the inferior colliculus of the rat did not differ

between neurons with characteristic frequencies ranging between 1 and 40 kHz. Schreiner and Urbas⁴² found, for neurons in the anterior auditory field of cat cortex, a small positive correlation between best modulation frequency and characteristic frequency with sinusoidal modulation, but no significant correlation when the modulating signal was a square wave. We did not measure MTFs at carrier frequencies above 250 Hz because diminishing response amplitudes necessitated an impractical measurement time. Nevertheless, animal data provide only little evidence for a general change of the upper slope of MTFs as carrier frequency changes.

The low-frequency slope of the MTF obtained in our study (6 dB/octave below 20 Hz; see Fig. 5) is flat compared to the high-frequency slope (18 dB/octave above 50 Hz). This shape is in contrast to bandpass-like MTFs found by Rees and Møller⁴⁰ in the inferior colliculus of the rat with a stimulus intensity of 60 dB. The MTFs obtained by Rees and Møller may have been influenced not only by the collicular origin of the auditory response, but also by the fact that MTFs were obtained from Fourier transform of correlograms between stimulus signal and period histograms of the response. For this calculation the assumption of a linear system is required which is not fulfilled, especially at low frequencies.

At low modulation frequencies the response waveform is periodic with the modulation frequency and consists of a number of distinguishable components. This results in an amplitude spectrum composed of harmonics of the modulation frequency, with maximum values in the 40-Hz range. It is rather unlikely that the response waveform to low modulation frequencies results from nonlinear distortions. More obviously it resembles an intrinsic waveform pattern that is triggered by the rising edge of the stimulus signal envelope. For modulation frequencies of 40 Hz and above, the SSR waveform is almost sinusoidal and follows the modulating waveform with some time delay. It may be possible that single periods of the modulated stimulus elicited transient responses. This would support the hypothesis of SSR generation by periodic superimposition of transient responses. This hypothesis was established first by Galambos,² who synthesized a 40-Hz response from repetitively superimposed middle latency responses that were evoked by short tone pulses presented at 10 per s. Azzena *et al.*¹⁰ confirmed this finding for the modulation frequency of 40 Hz but not for frequencies below and above 40 Hz. Our findings regarding the frequency-group delay IOC [Fig. 6(b)], which showed local maxima at 20 Hz (72 ms), 40 Hz (48 ms), and 80 Hz (26 ms) provides an important contribution to this discussion. An explanation of the group delay is that the group of frequencies centered around ω_0 is delayed by the amount of group delay τ , in the sense that their contribution to the impulse response is maximum at that instant.³⁴ Therefore, the transient N_a-P_a waves (20 and 30 ms latency) could relate to the 80-Hz SSR, the N_b-P_b waves (latency of 38 and 52 ms) to the 40-Hz SSR, and the P_1-N_1 waves to the 20-Hz SSR. This interpretation is in line with the hypothesis of generation of SSR by linear superimposition of subsequent transient response components.

On the other hand, if it is assumed that an enhanced

excitability for 40-Hz activity exists in some neural networks,⁴³ generation of SSR with a pronounced amplitude response around 40 Hz could be modeled by a damped oscillator, either linear or nonlinear. This model would necessarily contain one or more second-order components. A property of such a second-order linear system is that the phase response should show the steepest decrease, and therefore a maximum group delay, at the frequency of the response maximum. Indeed, the 20- and 40-Hz maxima of the group delay characteristic coincide with two peaks of the amplitude characteristic, and a third peak of the amplitude characteristic at 80 Hz might be blurred by its falling slope. Thus, the group delay characteristic provides data consistent with both hypotheses (linear superimposition and synchronization of intrinsic oscillations). It should be noted that these two hypotheses are not mutually exclusive.

The three distinct peaks of the modulation frequency-phase characteristic at 20, 40, and 80 Hz divide the frequency axis into three sections, a low-frequency section below 30 Hz, a mid range between 30 and 70 Hz, and an upper range above 70 Hz. At least for the carrier frequency of 250 Hz, this division is consistent with different perceptual categories within each frequency range. In the low-frequency range the amplitude-modulated tone is perceived as a beating sound, as roughness in the 30- to 70-Hz range, and as pitch in the upper-frequency range.

B. Stimulus intensity

The intensity-amplitude IOC obtained in this study suggests a stable causal system and is very similar to characteristics reported in previous studies.^{18,44,33} The saturation level of 70- to 80-dB sensation level which we observed agrees with a previous EEG study with AM sounds³⁸ modulated to the level of 60 dB. However, in contrast to stimulus intensity IOCs which have been reported for SSRs evoked by short tone bursts,¹⁸ we found evidence of saturation in the region of 90-dB sensation level. The reason could be that compared to short tone bursts, the power of the SAM tones is much higher due to the continuously presented carrier signal. This could cause habituation which prevents a further increase in SSR amplitude at stimulus intensities near 80–90 dB [Fig. 7(a)].

An extrapolation of the obtained intensity-amplitude IOC towards lower intensities crosses the zero-amplitude axis between 15- and 20-dB sensation level. This intensity can be interpreted as the threshold for elicitation of the SSR. This finding corresponds to thresholds previously reported by Stürzebecher⁴⁵ (10 dB above behavioral threshold), Szyter⁴⁶ (15 dB), Rees³⁸ (15 dB), and Rodriguez³³ (3–20 dB).

The intensity-phase IOC [Fig. 7(b)] can be explained by the threshold model of latency.⁴⁷ This model assumes that a neuron's onset response is triggered whenever the signal reaches a fixed threshold amplitude. If the stimulus signal has a rising edge with a constant form, as in the case of the cosine-shaped envelope of an SAM tone, the threshold will be reached earlier for a higher intensity than for a lower intensity. The argument of Heil^{48,49} that the latency depends mostly on the acceleration of the envelope rather than on

amplitude, does not change the intensity-latency IOC expected in the case of an SAM signal. This is true because the second derivative of the envelope which represents its acceleration has the same shape, however with inverted sign. The observed latency shift of about 6 ms, which is the half of the rising edge of the envelope, fits very well to the model mentioned above.

C. Modulation depth

The modulation depth-amplitude IOC obtained in this study [Fig. 7(c)] agrees with results obtained by Rees *et al.*³⁸ in an EEG study of SAM sounds in which SSR amplitude increased linearly with modulation depth on a logarithmic scale. In contrast, Kuwada *et al.*⁴⁴ reported a linear relation between modulation depth and response amplitude from a single subject. The observed similarity between the modulation depth-amplitude IOC and the intensity-amplitude IOC shown in Fig. 7(a) may be explained by viewing the stimulus signal as the sum of two terms

$$y(t) = m \cdot a \cdot \sin(\omega_c t) \cdot (1 - \cos(\omega_m t)) \\ + (1 - m) \cdot a \cdot \sin(\omega_c t). \quad (3.1)$$

The first term is an SAM signal with 100% modulation depth, whereas the second term is a sine wave signal with constant amplitude. Only the effect of the first term contributes to a SSR at the modulation frequency, and no response will be evoked by the second term. The amplitudes of both terms change with variation of m . When the stimulus signal is only the first term, variation of m is obviously equivalent to the investigation of the effect of overall intensity variation. Therefore, in Fig. 7(c), m is shown on a logarithmic scale. The resulting modulation depth-amplitude IOC is almost linear with a steeper slope than observed from the overall intensity-amplitude IOC. This steeper slope can be interpreted as the influence of the second term of the stimulus signal, which gives amplitude increases with decreasing modulation depth. The modulation depth-phase IOC is completely different in comparison to the intensity-phase IOC and shows a reversed relation between latency and intensity of the relevant part of the stimulus signal. These findings are completely in line with a phase characteristic presented by Kuwada *et al.*⁴⁴

D. Carrier frequency

The SSR frequency-amplitude IOC [Fig. 7(e)], for which amplitude decreased by a factor of 2.8 with frequency increasing from 250 to 4000 Hz in this study, has been reported in the EEG literature in experiments using short tone-burst stimulation. Galambos² reported an amplitude decrease by a factor of about 2 to 3 for three subjects when carrier frequency increased from 250 to 5000 Hz. This result was attributed to activation of larger portions of the basilar membrane by low-frequency tones. Stapells¹⁸ also obtained an amplitude decrease by a factor of 1.4 when increasing the carrier frequency from 500 to 4000 Hz. In an EEG study with short tone bursts (4-ms rise and fall time and a 2-ms plateau at a rate of 40/s), Rodriguez *et al.*³³ found the SSR amplitude decreased by a factor of 2.33 when frequency in-

creased from 500 to 4000 Hz. Following the hypothesis of superimposition of middle latency responses (MLR), Rodriguez *et al.* explained the amplitude effect by suggesting that frequency-dependent latency variations of the different MLR components may have resulted in perfect aggregation of the SSR at low frequencies and less effective summation at higher frequencies. Rodriguez *et al.* noted especially the contribution of the frequency sensitive wave V of the brainstem responses to the MLR. However, the contribution of brainstem responses to the SSR can be excluded from the results of the present study, because the MEG recordings were not sensitive enough to see brainstem activity. The results of our study are in line with findings of a previous study by Pantev *et al.*¹⁵ of the steady-state field (SSF). Pantev *et al.* reported a decrease by a factor of 2 for the global field power and the strength of the cortical source of the SSF in the frequency range from 250 to 4000 Hz. The same amplitude effect was reported by Kuwada *et al.*⁴⁴ for SSRs measured by EEG. Thus, the behavior of the frequency-amplitude IOC is consistent in both EEG and MEG recordings.

The variation in the amplitude of the SSR with carrier frequency certainly reflects the tonotopic organization of the SSR. In this respect, the cortical sources of steady-state responses recorded in this study were found to be tonotopically organized. This tonotopic organization was most pronounced in the mediolateral direction and spanned a distance averaging 0.5 cm over the eight subjects for a frequency variation of 250 to 4000 Hz. This result, which corroborates an earlier report by Pantev *et al.*,¹⁵ means that the magnetic field power of a deeper source related to higher stimulus frequency is smaller than the magnetic field power of a laterally located source which is related to low stimulus frequency. The source space projections in this study, however, were calculated for a fixed estimation of dipole position which corresponded to the median of source parameters in the relevant experimental condition. The estimated coordinates matched exactly the 1000-Hz source of Pantev *et al.*,¹⁵ and consequently the SSR amplitude for 1000 Hz was correctly estimated. Under the assumption of tonotopic organization, the source depth of the 250-Hz response was estimated to be too deep, which results in an overestimate of the 250-Hz SSR amplitude. In contrast, the 4000-Hz amplitude was underestimated. In order to evaluate this amplitude error, the source coordinates were systematically varied in all directions and the corresponding dipole moments were recalculated. This simulation showed that a 0.5 cm variation in the mediolateral direction would introduce a factor of no more than 1.3 in the amplitude of the equivalent source dipole. Thus, even accounting for the influence of tonotopy, the factor of greater than 2 obtained in this study for carrier frequency cannot be sufficiently explained.

In the frequency range from 250 to 4000 Hz, the SSR phase increases by $\pi/2$ as shown in Fig. 7(f). This corresponds to a 6.25-ms longer latency for the 250-Hz response compared to 4000 Hz. From EEG studies, Galambos² reported a latency shift of 6 ms, 5 ms of which he attributed to frequency-dependent traveling time along the basilar membrane. Rodriguez³³ as well reported a latency shift of 6 ms

but estimated that only 2–3 ms of the observed delay could be explained at the cochlear level.

IV. SUMMARY

Amplitude-modulated tones elicit cortical activity at the modulating frequency and its harmonics. Using MEG recordings, the SSR signal was detected with high precision and was separated from other brain sources. SSR amplitude decreased linearly when either stimulus intensity or modulation depth decreased on a logarithmic scale. In contrast, the phase lag between the SSR and the stimulus signal envelope decreased when the intensity increased but changed in the opposite direction when the modulation depth increased. A reduction of SSR amplitude was found for higher carrier frequencies, which is consistent with recently reported EEG recordings. A modulation transfer function was obtained from measurements of SSR amplitude when modulation frequency was incremented in fine steps between 10 and 98 Hz. The obtained MTF resembled psychophysical functions relating AM perception when pitch perception is excluded. From the SSR phase-modulation frequency characteristic, a group delay characteristic was derived which showed three distinct peaks with decreasing time delay as the modulation frequency increased.

ACKNOWLEDGMENTS

This work was supported by grants from the Deutsche Forschungsgemeinschaft (No. Pa392/7-1). The authors thank Karin Berning for assistance and Dr. Scott Makeig for helpful comments.

¹J. S. Buchwald and C. M. Huang, "Far-field acoustic response: origins in the cat," *Science* **189**, 382–384 (1975).
²R. Galambos, S. Makeig, and P. J. Talmachoff, "A 40-Hz auditory potential recorded from the human scalp," *Proc. Natl. Acad. Sci. USA* **78**, 2643–2647 (1981).
³D. Regan, "Comparison of transient and steady-state methods," *Ann. (N.Y.) Acad. Sci.* **388**, 45–71 (1982).
⁴D. Regan, *Human Brain Electrophysiology: Evoked Potentials and Evoked Magnetic Fields in Science and Medicine* (Elsevier, New York, 1989).
⁵D. S. Barth and S. Di, "Three-dimensional analysis of auditory-evoked potentials in rat neocortex," *J. Neurophysiol.* **64**, 1527–1536 (1990).
⁶M. N. Franowicz and D. S. Barth, "Comparison of evoked potentials and high-frequency (gamma-band) oscillating potentials in rat auditory cortex," *J. Neurophysiol.* **74**, 96–112 (1995).
⁷B. H. Gaese and J. Ostwald, "Temporal coding of amplitude and frequency modulation in the rat auditory cortex," *Eur. J. Neurosci.* **7**, 438–450 (1995).
⁸J. P. Mäkelä, G. Karmos, M. Molnar, V. Csepe, and I. Winkler, "Steady-state responses from the cat auditory cortex," *Hear. Res.* **45**, 41–50 (1990).
⁹M. Yoshida, L. D. Lowry, J. J. C. Liu, and K. Kaga, "Auditory 40-Hz responses in the guinea pig," *Am. J. Otolaryngol.* **5**, 404–410 (1984).
¹⁰G. B. Azzena, C. Conti, R. Santarelli, F. Ottaviani, G. Paludetti, and M. Maurizi, "Generation of human auditory steady-state responses (SSRs), I: Stimulus rate effects," *Hear. Res.* **83**, 1–8 (1995).
¹¹N. Forss, J. P. Mäkelä, L. McEvoy, and R. Hari, "Temporal integration and oscillatory responses of the human auditory cortex revealed by evoked magnetic fields to click trains," *Hear. Res.* **68**, 89–96 (1993).
¹²R. Hari, M. Hämäläinen, and S. L. Joutsiniemi, "Neuromagnetic steady-state responses to auditory stimuli," *J. Acoust. Soc. Am.* **86**, 1033–1039 (1989).
¹³M. Joliot, U. Ribary, and R. Llinas, "Human oscillatory brain activity

near 40 Hz coexists with cognitive temporal binding," *Proc. Natl. Acad. Sci. USA* **91**, 11748–11751 (1994).
¹⁴C. Pantev, T. Elbert, S. Makeig, S. Hampson, C. Eulitz, and M. Hoke, "Relationship of transient and steady-state auditory evoked fields," *Electroencephalogr. Clin. Neurophysiol.* **88**, 389–396 (1993).
¹⁵C. Pantev, L. E. Roberts, T. Elbert, B. Roß, and C. Wienbruch, "Tonotopic organization of the sources of human auditory steady-state responses," *Hear. Res.* **101**, 62–74 (1996).
¹⁶G. Plourde, D. R. Stapells, and T. W. Picton, "The human auditory steady-state evoked potentials," *Acta Oto-Laryngol. Suppl.* **491**, 153–159 (1991).
¹⁷R. Santarelli, M. Maurizi, G. Conti, F. Ottaviani, G. Paludetti, and V. E. Pettorossi, "Generation of human auditory steady-state responses (SSRs). II. Addition of responses to individual stimuli," *Hear. Res.* **83**, 9–18 (1995).
¹⁸D. R. Stapells, D. Linden, J. B. Suffield, G. Hamel, and T. W. Picton, "Human auditory steady state potentials," *Ear Hear.* **5**, 105–113 (1984).
¹⁹A. A. Borbély, "Changes in click evoked responses as a function of depth in auditory cortex of the rat," *Brain Res.* **21**, 217–247 (1970).
²⁰G. Conti, R. Santarelli, C. Grassi, F. Ottaviani, and G. B. Azzena, "Auditory steady-state responses to click trains from the rat temporal cortex," *Clin. Neurophysiol.* **110**, 62–70 (1999).
²¹G. V. Simpson and R. T. Knight, "Multiple brain systems generating the rat auditory evoked potential. I. Characterization of the auditory cortex response," *Brain Res.* **602**, 240–250 (1993).
²²L. S. Lee, H. Lueders, D. S. Dinner, R. P. Lesser, J. Hahn, and G. Klem, "Recording of auditory evoked potentials in man using chronic subdural electrodes," *Brain Res.* **107**, 115–131 (1984).
²³C. Liégeois-Chauvel, A. Musolino, J. M. Badier, P. Marquis, and P. Chauvel, "Evoked potentials recorded from the auditory cortex in man: evaluation and topography of the middle latency components," *Electroencephalogr. Clin. Neurophysiol.* **92**, 204–214 (1994).
²⁴B. W. Johnson, H. Weinberg, U. Ribary, D. O. Cheyne, and R. Ancill, "Topographic distribution of the 40 Hz auditory evoked-related potential in normal and aged subjects," *Brain Topogr.* **1**, 117–121 (1988).
²⁵J. P. Mäkelä and R. Hari, "Evidence for cortical origin of the 40 Hz auditory evoked response in man," *Electroencephalogr. Clin. Neurophysiol.* **66**, 539–546 (1987).
²⁶G. L. Romani, S. J. Williamson, L. Kaufman, and D. Brenner, "Characterization of the Human Auditory Cortex by the Neuromagnetic Method," *Exp. Brain Res.* **47**, 381–393 (1982).
²⁷R. C. Oldfield, "The Assessment and analysis of handedness: The Edinburgh inventory," *Neuropsychologica* **9**, 97–113 (1971).
²⁸J. Jerger, R. Chmiel, J. D. J. Frost, and N. Coker, "Effect of sleep on the auditory steady state evoked potential," *Ear Hear.* **7**, 240–245 (1986).
²⁹M. Hämäläinen, R. Hari, R. J. Ilmoniemi, J. Knuutila, and O. Lounasmaa, "Magnetoencephalography – theory, instrumentation, and applications to noninvasive studies of the working human brain," *Rev. Mod. Phys.* **65**, 413–497 (1993).
³⁰R. J. Ilmoniemi, S. J. Williamson, and W. E. Hostetler, "New method for the study of spontaneous brain activity," in *Biomagnetism '87*, edited by K. Atsumi, M. Kotani, S. Ueno, T. Katila, and S. J. Williamson (Tokyo Denki University Press, Tokyo, 1987), pp. 182–185.
³¹S. E. Robinson and D. F. Rose, "Current source image estimation by spatially filtered MEG," in *Biomagnetism: Clinical Aspects*, edited by M. Hoke, S. Erné, Y. Okada, and G. Romani (Excerpta Medica, Amsterdam, 1992), pp. 761–765.
³²S. E. Robinson, "Theory and properties of lead field synthesis analysis," in *Advances in Biomagnetism*, edited by S. Williamson, M. Hoke, G. Stroink, and M. Kotani (Plenum, New York, 1989), pp. 599–602.
³³R. Rodriguez, T. Picton, D. Linden, G. Hamel, and G. Laframboise, "Human auditory steady state responses: Effects on intensity and frequency," *Ear Hear.* **7**, 300–313 (1986).
³⁴L. Zadeh and C. A. Desoer, *Linear System Theory* (McGraw-Hill, New York, 1963).
³⁵A. C. Davison and D. V. Hinkley, *Bootstrap Methods and their Application* (Cambridge University Press, Cambridge, England, 1997).
³⁶N. F. Viemeister, "Temporal modulation transfer functions based upon modulation thresholds," *J. Acoust. Soc. Am.* **66**, 1364–1380 (1979).
³⁷E. Terhardt, "On the perception of periodic sound fluctuations (roughness)," *Acustica* **30**, 201–213 (1974).
³⁸A. Rees, G. G. R. Green, and R. H. Kay, "Steady-state evoked responses to sinusoidally amplitude-modulated sounds recorded in man," *Hear. Res.* **23**, 123–133 (1986).

- ³⁹R. D. Frisina, R. L. Smith, and S. C. Chamberlain, "Encoding of amplitude modulation in the gerbil cochlear nucleus. I. A hierarchy of enhancement," *Hear. Res.* **44**, 99–122 (1990).
- ⁴⁰A. Rees and A. R. Møller, "Stimulus properties influencing the responses of inferior colliculus neurons to amplitude-modulated sounds," *Hear. Res.* **27**, 129–143 (1987).
- ⁴¹C. E. Schreiner and J. V. Urbas, "Representation of amplitude modulation in the auditory cortex of the cat. II. Comparison between cortical fields," *Hear. Res.* **32**, 49–64 (1988).
- ⁴²C. E. Schreiner and J. V. Urbas, "Representation of amplitude modulation in the auditory cortex of the cat. I. The anterior auditory field (AAF)," *Hear. Res.* **21**, 227–241 (1986).
- ⁴³E. Basar, R. Rosen, C. Basar-Eroglu, and F. Greitschus, "The associations between 40 Hz-EEG and the middle latency response of the auditory evoked potential," *Int. J. Neurosci.* **33**, 103–116 (1987).
- ⁴⁴S. Kuwada, R. Batra, and V. L. Maher, "Scalp potentials of normal and hearing-impaired subjects in response to sinusoidally amplitude-modulated tones," *Hear. Res.* **21**, 179–192 (1986).
- ⁴⁵E. Stürzebecher, W. Kühne, and H. Berndt, "Detectability of the acoustically evoked composite response (40 Hz potential) near threshold," *Scand. Audiol.* **14**, 23–25 (1985).
- ⁴⁶W. Szyfter, R. Dauman, and R. C. de Sauvage, "40 Hz middle latency responses to low frequency tone pips in normal hearing adults," *J. Otolaryngol.* **13**, 275–280 (1984).
- ⁴⁷D. P. Phillips and S. E. Hall, "Response timing constraints on the cortical representation of sound time structure," *J. Acoust. Soc. Am.* **88**, 1403–1411 (1990).
- ⁴⁸P. Heil, "Auditory cortical onset responses revisited. I. first-spike timing," *J. Neurophysiol.* **77**, 2616–2641 (1997).
- ⁴⁹P. Heil, "Auditory cortical onset responses revisited. II. response strength," *J. Neurophysiol.* **77**, 2642–2660 (1997).